Preprints.org

Article

Not peer-reviewed version

Improving the Luminescence Performance of Monolayers MoS2 by Doping Multiple Metal Elements with CVT Method

Bojin Zhao , Zongju Huo , Lujie Li , Hongjun Liu , Zhanggui Hu , Yicheng Wu , Hailong Qiu *

Posted Date: 3 August 2023

doi: 10.20944/preprints202308.0336.v1

Keywords: Doping; MoS2; CVT.

Preprints.org is a free multidiscipline platform providing preprint service that is dedicated to making early versions of research outputs permanently available and citable. Preprints posted at Preprints.org appear in Web of Science, Crossref, Google Scholar, Scilit, Europe PMC.

Copyright: This is an open access article distributed under the Creative Commons Attribution License which permits unrestricted use, distribution, and reproduction in any medium, provided the original work is properly cited.

Preprints (www.preprints.org) | NOT PEER-REVIEWED | Posted: 3 August 2023 doi:10.20944/preprints202308.0336.v1

Disclaimer/Publisher's Note: The statements, opinions, and data contained in all publications are solely those of the individual author(s) and contributor(s) and not of MDPI and/or the editor(s). MDPI and/or the editor(s) disclaim responsibility for any injury to people or property resulting from any ideas, methods, instructions, or products referred to in the content.

Article

Improving the Luminescence Performance of Monolayers MoS_2 by Doping Multiple Metal Elements with CVT Method

Bojin Zhao [1], Zongju Huo [1], Zhao Ma [1], Hongjun Liu [1], Zhanggui Hu [1], Yicheng Wu [1] and Hailong Qiu [1,*]

[1] Tianjin Key Laboratory of Functional Crystal Materials, Institute of Functional Crystal, Tianjin University of Technology, Tianjin 300384, China

* Correspondence: qiu@tjut.edu.cn

Abstract: Two-dimensional (2D) transition metal dichalcogenides (TMDCs) draw much attention as critical semiconductor materials for 2D, optoelectronic, and spin electronic devices. Although controlled doping of 2D semiconductors can also be used to tune their bandgap and type of carrier and further change their electronic, optical, and catalytic properties, it remains an ongoing challenge. Here, we successfully doped a series of metal elements (including Hf, Zr, Gd, Dy) into the monolayers MoS_2 through a single-step chemical vapor transport (CVT), and the atomic embedded structure is confirmed by scanning transmission electron microscope (STEM) with a probe corrector measurement. In addition, the host crystal is well preserved, and no random atomic aggregation is observed. More importantly, adjusting the band structure of MoS_2 enhanced fluorescence and carrier effect. This work provides a growth method for doping nonlike elements into 2D MoS_2 and potentially many other 2D materials to modify their properties.

Keywords: doping; MoS_2; CVT

1. Introduction

Two-dimensional (2D) transition metal dichalcogenides (TMDCs) materials are considered to have great potential for application in fields such as integrated circuits, field-effect transistors (FET), and optoelectronic devices[1-3]. In order to expand its application circumstance, doping can be used to regulate the performance of TMDC materials. For instance, doping in TMDCs has the potential to modulate their charge carrier concentration, phase, electronic and optical band structures, and magnetic properties and may give TMDCs new properties and functionalities for various applications[4-8].

However, the current doping method of monolayer MoS_2 will cause lattice distortion and uneven doping[9-11]. For example, Physical vapor deposition (PVD) and chemical vapor deposition (CVD) have poor crystallization quality and uniformity. On the other hand, note that previous achievements in metal substitutional doping of TMDCs are primarily limited in the metal substitutional doping of TMDCs is mainly limited to part of the transition metal elements (e.g., Mo, W, Re, Nb, which can be referred to like-elements) that form corresponding species in the TMDC family, such as MoS_2, WSe_2, ReS_2, and NbS_2[12-13]. For example, Suh et al[14]. found that the substitutional doping of MoS_2 with Nb leads to its structural transformation from the 2H to the 3R phase.

Nevertheless, the doping of unlike elements still poses significant challenges. On the contrary, recent theoretical research has found that elements such as Cr, Mn, Fe, etc., if doped into TMDC materials, will greatly alter the properties of TMDC and endow the materials with unique characteristics, such as dilute magnetism and self-spintronic applications[15-17]. But successful examples are rarely reported. For example, it was reported that Er-doped MoS_2 thin films were obtained by depositing Er onto Mo-thin films and then vulcanizing them, and their optical properties

© 2023 by the author(s). Distributed under a Creative Commons CC BY license.

Preprints (www.preprints.org) | NOT PEER-REVIEWED | Posted: 3 August 2023 doi:10.20944/preprints202308.0336.v1

were improved[18]. However, this method is not generalizable and requires strict experimental conditions. The domain size of Er-doped MoS_2 thin films grown through sulfurization is usually relatively small. This requires a doping method that can have universality and ensure the production of high-quality TMDC materials, opening up ideas for this field.

Here, we use MoS_2 as the representative material of TMDCs and synthesize high-quality monolayer MoS_2 using chemical vapor transport (CVT) in a high vacuum-sealed environment. Based on further improving the process, a one-step CVT method was implemented to achieve the doping of IVB and VB transition metal elements, introducing foreign defects to enrich the electronic energy level structure of MoS_2 itself and improving the luminescence performance of monolayer MoS_2 crystal. On the other hand, the doping of lanthanide elements was also achieved using this method, and fluorescence-enhanced MoS_2 crystals doped with lanthanide elements were obtained. The band structure of MoS_2 was changed by using the rich electronic energy level of rare earth elements. It finds that the fluorescence of MoS_2 markedly enhances after doping[19-21]. Moreover, the carrier lifetime was substantially prolonged by the kinetic test. These works are of great significance for further research on 2D MoS_2 optoelectronic devices and FET transistors[22].

2. Materials and Methods

Sample preparation: The Zr, Hf, Gd, and Dy-doped MoS_2 monolayers were synthesized by the CVT growth method. First, MoO_3 (Alfa Aesar, 99.7%, ≈ 2.3 mg), ZrO_2 (Alfa Aesar, 99.99%, ≈ 0.60 mg), HfO_2 (Alfa Aesar, 99.99%, ≈ 1.01 mg), $GdCl_3$ (Alfa Aesar, 99.99%, ≈ 1.22 mg), $DyCl_3$ (Alfa Aesar, 99.99%, ≈ 1.25 mg), S (Alfa Aesar, 99.7%, ≈ 0.40 mg), and transport agent of iodine (Alfa Aesar, 99.7%, ≈ 3.00 mg) powers were mixed and loaded into a quartz ampule at one end. The mica substrate and raw materials are placed at both ends of the quartz tube and separated by the necking of the quartz tube. Afterwards, vacuum the quartz tube to $3\text{-}5\times10^{-4}$ Pa and sealed. The experiment used a single temperature zone tube furnace, with a high temperature zone in the middle and low temperature zones at both ends. The raw material area in the sealed quartz tube is placed in the high-temperature zone, and the substrate area (growth zone) is placed in the low-temperature zone. Set the procedure to heat up to 850 ℃ at 40 ℃/min, hold for 0.5-2 h, and then air cooled to room temperature.

Transfer Method: Use a homogenizer to adsorb the doped monolayer MoS_2 film and rotate it at 3000 rpm for 20 seconds while dripping PMMA solution onto the surface of the film. Then remove the sample and place it on a heating plate to heat at 80 ℃ for 8-10 minutes to cure. After cooling the sample to room temperature, the PMMA-deposited MoS_2 film and substrate were separated by soaking in deionized water. Finally, the thin film is transferred to the desired substrate and annealed at 70 ℃ for 2 h to firmly adhere to the substrate. The PMMA film is then washed or soaked with acetone to dissolve and release the MoS_2 film onto the target substrate.

Optical Spectroscopy Measurement: Commercial Confocal microscopy (WITec Alfa-300) is used to test PL and Raman data. The testing conditions are room temperature, laser wavelength of 532 nm, and spatial resolution of 2 μm. This microscope worked in reflection mode, and the signal was detected using an electrically cooled charge-coupled device camera.

The TR spectrum was obtained through testing using a self-built ultra-fast pump-probe spectroscopy system in the laboratory. A homemade microscope was connected to the system to realize micro-resolution. A Yb: KGW laser (Pharos, Light Conversion Ltd., a repetition rate of 100 kHz; pulse width of 120 fs) with a working wavelength of 1030 nm was used as the light source. The laser output beam is divided into pump light and probe light during the testing process. Pump light is used to generate pump pulses (315-2600 nm) to pump the sample. The probe light passes through the time delay line and focuses on the YAG crystal to produce a continuum pulse to probe the dynamics after pumping. After filtering the pump pulse using a long-wave filter, the reflection spectrum is collected with a complementary metal-oxide-semiconductor detector. The TR signal is calculated as $\Delta R/R$ = (Rpump-on-Rpump-off)/Rpump-off, where Rpump-on and Rpump-off are the reflection detection signals with and without pump excitation.

Characterization: The optical micrograph of Hf, Zr, Dy, and Gd-doped MoS_2 was taken and observed through Olympus BX 51M. XPS data were collected using Thermo Scientific

Preprints (www.preprints.org) | NOT PEER-REVIEWED | Posted: 3 August 2023 doi:10.20944/preprints202308.0336.v1

ESCALAB250Xi, and all peaks would be calibrated with C1s peak binding energy at 284.8 eV for adventitious carbon. STEM images of doped MoS_2 were obtained using Titan 60-300 at 200 kV.

3. Results and Discussion

We chose the Hf element as the representative element for monolayer MoS_2 crystals doped with transition metal materials, using the CVT method of a sealed quartz tube. The mixture of MoO_3/HfO_2/S/I_2 powers and growth mica substrate were placed on both ends of the quartz tube, as shown in Figure 1a. When using CVT method to obtain ultra-thin MoS_2, it is essential to use a way to reduce the transport efficiency of the transport agent. The specific implementation method is to reduce the size of the transport channel between the raw material and substrate (as shown in Figure 1a). This design can separate the substrate and raw materials and slow down the transport rate, thereby controlling the film size and thickness[23]. The final obtained model structure of Hf-doped MoS_2 is a 2H-MoS_2 structure where Hf replaces Mo atoms.

Figures 1c,d, and e show optical micrographs, Raman, and PL spectra of Hf-doped monolayer MoS_2 crystal, respectively. From the optical photo, it can be seen morphology of MoS_2 after doping remains almost unchanged, maintaining the growth morphology of pure MoS_2. In addition, Figure 1d shows the two characteristic Raman vibration modes of E^1_{2g} and A_{1g} mode related to the out-of-plane vibration. The similar Raman spectra also confirm that the lattice has no significant changes after doping, except for the collective red-shift of Raman peak positions caused by lattice distortion after atomic substitution. The Raman spectrum characterization measured a 19 cm^{-1} difference in the A_{1g} and E^1_{2g} vibration peak position of doped MoS_2[24-25], consistent with the Raman peak position difference between monolayer MoS_2. The Raman Mapping diagram in the illustration also indicates the uniformity of crystal quality after doping. The steady-state PL spectra were collected on the pristine and Hf-doped MoS_2 monolayers under the same conditions at room temperature, as listed in Figure 1e. The test shows that the PL intensity of Hf-doped monolayer MoS_2 is stronger than that of pure MoS_2, which is about five times stronger. Additionally, the PL peak position is slightly blue-shifted due to the lattice distortion and bandgap changes caused by doping. Simultaneously, the luminescence peak of PL also has a narrow half-peak width, indicating the uniformity of luminescence quality[26-27]. There, we believe that doping the Hf element introduces the electronic energy level of the Hf element, which enriches the electronic structure of MoS_2.

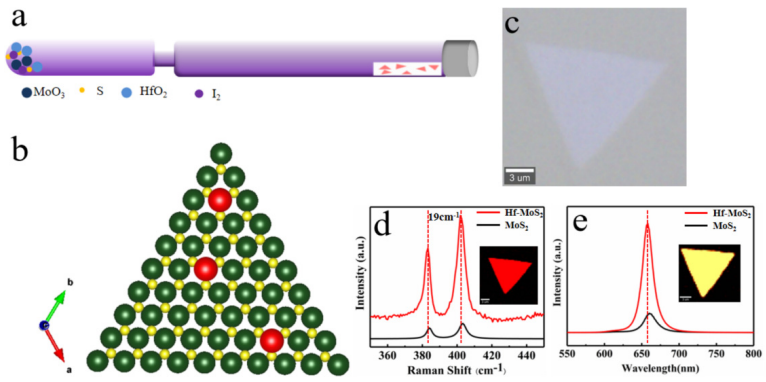

Figure 1. The principle and optical characterization of Hf-doped MoS_2 monolayer synthesized by CVT method. (a) Simulation diagram of Hf-doped monolayer MoS_2 grown by CVT method. (b) Schematic atomic model of Hf-doped MoS_2 in top view. (c) Microscopic optical photos of Hf-doped monolayer MoS_2. (d) (e) Raman/PL spectra of Hf-MoS_2 and pure MoS_2 were obtained with a 532 nm laser. Inset: Spatially resolved Raman/PL intensity mapping at 385 cm^{-1}/657 nm for the Hf-MoS_2 monolayer.

HAAD-STEM can distinguish different atoms according to different brightness, which is caused by different atomic numbers (S (Z=16), Mo (Z=42), and Hf (Z=72)). Based on this, we marked the position occupied by Hf doping in the MoS_2 monolayer with red circles in Figure 2a. Simultaneously, the plane spacing between two adjacent (100) faces is 0.28 nm, which is consistent with the data of pure monolayer MoS_2. But, measurement found that the distance between two adjacent Mo atoms

Preprints (www.preprints.org) | NOT PEER-REVIEWED | Posted: 3 August 2023 doi:10.20944/preprints202308.0336.v1

was 0.32 nm, and compared with pure phase MoS_2, the distance between faces and atoms increased. This is because the Hf atom is much larger than the Mo atom, leading to slight lattice distortion in MoS_2.

On the other hand, it proves that the Hf atom has successfully embedded in the lattice of MoS_2, replacing the position of Mo atoms, which is consistent with HAADF-STEM testing. Furthermore, in Figure 2b, the highlighted area in Figure 1a was enlarged, and a clear distinction between light and dark can be seen. In addition, the illustration in Figure 2a also shows the uniformity and high quality of the thin film material[28].

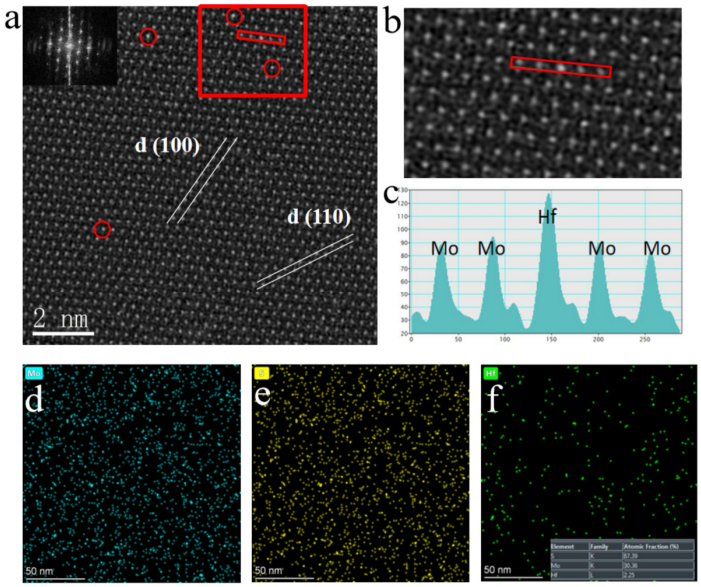

Figure 2. STEM and EDS test results of Hf-doped monolayer MoS_2.. (a) Transmission electron microscope with a probe corrector (STEM) imaging. Inset: the corresponding FFT-diffraction patterns. (b) An enlarged view of the red rectangular area in (a). (c) The intensity line profile corresponding to the marked area in (b). (e-g) Spatially resolved EDS maps collected from the same area in a Hf-MoS_2 monolayer for the Mo-K, S-K, and Hf-L lines, respectively.

The profile of the intensity line in Figure 2c corresponds to the selected area in Figure 2b, where Hf and Mo atoms are marked. All the dots at Mo atom sites show similar contrast except for the bright sites for Hf atoms, suggesting that almost no Mo atom vacancies are found on the measured surface[7,29]. Another noteworthy phenomenon is that the strength near the Hf atom substituting the Mo atom is different from that near the Mo atom in other regions (Figure 2c). We supposed that this is due to the generation of new bonding oxygen atoms near the doped Hf atom and the formation of a new O-Hf-S structure by replacing the S atom. Furthermore, EDS spectrum mapping shows that Hf is evenly distributed among atoms in the sample, which a doping amount of approximately 1:15 compared to the Mo element (Figure 2f, illustration). Moreover, the sum of the ratio of the Mo element to the S element is about 1:2, proving that the Hf element replaces the Mo element. Moreover, the absence of noticeable lattice distortion and the presence of Mo vacancies are necessary proof for proving the feasibility of this doping process[30-31].

The femtosecond pump-probe is an essential tool for studying the carrier dynamics of Hf-doped MoS_2 monolayers (please refer to the Materials and Methods section for detailed testing information). Firstly, we tested the 2D profile of transient reflection (TR) spectra of the Hf-doped MoS_2 monolayer at room temperature with the excitation power of 2 μw under a 530 nm laser. Figure 3b shows the TR spectrum of A exciton resonance with a 4.2 ps time delay extracted from Figure 3a. Two peaks in each TR spectrum correspond to the A and B excitons of the Hf-doped MoS_2 monolayer, which are much stronger than those of pure MoS_2, corresponding to the phenomenon of luminescence enhancement in the PL spectrum. Therefore, we collected the TR kinetic decay curves of A-exciton resonance in Hf-doped MoS_2, as shown in Figure 3c. Analyze the kinetic decay curves through tri-exponentially fitted

Preprints (www.preprints.org) | NOT PEER-REVIEWED | Posted: 3 August 2023 doi:10.20944/preprints202308.0336.v1

(the results are listed in Table 1). The fitting results indicate that the relaxation lifetime τ_1 has increased from 0.91 ps to 2.14 ps after doping, which is believed to be due to the additional defect scattering of hot carriers caused by Hf doping, thereby prolonging the relaxation time. More importantly, the lifetime τ_2 representing the radiative recombination process has also significantly increased. According to the previous report[32-34], the photoluminescence quantum yield (PLQY) enhancement of two different radiation processes can be roughly estimated by the following equation:

$$\eta = \frac{\bar{\tau}_D}{\bar{\tau}_P}$$

Here, $\bar{\tau}_D$ and $\bar{\tau}_P$ correspond to the average exciton lifetime of doped and undoped monolayer MoS_2, respectively. Based on the previous work of our research group[7], substituting τ_2 to calculate PLQY enhancement instead of average lifetime. The calculated value of η is approximately 1.67, confirming the previously observed phenomenon of PL enhancement after Hf doping. It is worth noting that the calculated value of η based on this formula is an estimated value, far less than the five times luminescence enhancement obtained through PL testing, which is related to the testing mechanism. TR spectrum is an absorption spectrum collected through a pump probe, while PL spectrum is based on the spectrum obtained by a streak camera, which provides more accurate data compared to the former. On the other hand, the TR detection system is a platform built by our laboratory, and its collection efficiency is weaker than commercial confocal microscopy detection platforms. Thus, the PLQY enhancement, η is underestimated.

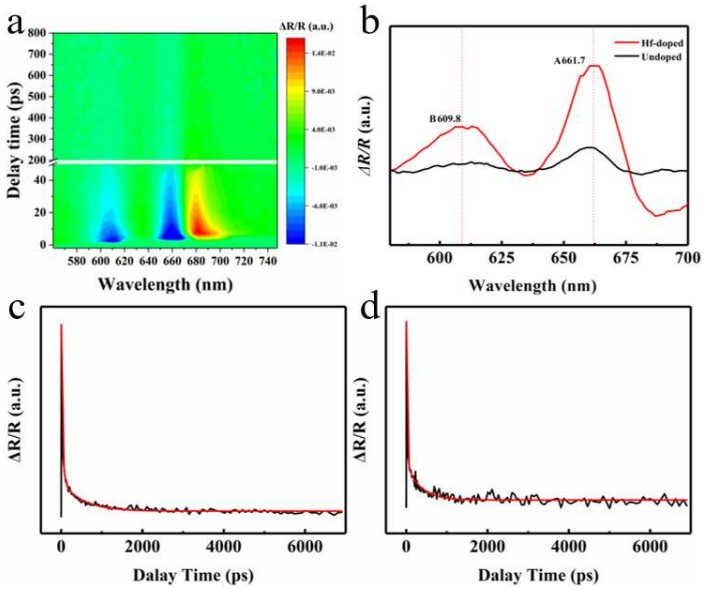

Figure 3. Time-resolved dynamics of the Hf-doped. (a) TR contour plot of Hf-doped MoS_2 monolayer on a mica substrate. (b) TR spectra extracted from (a) with the delay of 4.2 ps under the 532 nm laser excitation. (c, d) The TR kinetic curves of exciton resonance of A and B obtained through a triexponential fitting were extracted from (b).

Table 1. Tri-exponentially fitted Lifetimes results of A-exciton resonance for the Hf-doped and undoped monolayer MoS_2.

Exciton	Monolayer	τ_1 (ps)	τ_2 (ps)	τ_3 (ps)
A	Pristine	0.91	24.11	390.08
	Doped	2.14	40.18	522.78

Furthermore, the radiation efficiency is positively correlated to the densities of electrons in the conduction band and holes in the valance band. During the EEA process (τ_3), the exciton-scattering makes one non-radiatively recombine, passing the energy to the other exciton. The additional energy

Preprints (www.preprints.org) | NOT PEER-REVIEWED | Posted: 3 August 2023 doi:10.20944/preprints202308.0336.v1

promotes the residual exciton to become a free carrier. Therefore, the increase in carrier density caused by doping is another key factor that enhances PL in addition to PLQY. From Table 1, we can intuitively see that the lifetime τ_3 of the doped EEA process is much enhanced compared to the original monolayer MoS_2, and a longer lifetime promotes radiation recombination and improves PL intensity[35-37]. Based on the above discussion, we believe that the enhancement of PL by decay lifetime is crucial.

From the perspective of material structure, combining STEM images and XPS test results (Figure S1, supporting literature), we assume that the doping process introduces doping elements and some oxygen atoms, which can repair vacancies in monolayer MoS_2 while suppressing nonradiative recombination, improving carrier lifetime and enhancing PL. The absence of Mo and S vacancies in the STEM test image in Figures 2a-c is also substantial proof. Moreover, the O-Hf-S unit and Hf atoms mentioned earlier can also improve the interaction between monolayer MoS_2 and mica substrate, stabilizing excitons and leading to longer exciton lifetimes, ultimately achieving enhanced PL luminescence[38].

Unlike the IVB group elements, the sizeable atomic radius of rare earth elements will cause more significant lattice distortion of monolayer MoS_2 crystals after doping. On this basis, high-quality lanthanide (Gd, Dy) doped monolayer MoS_2 crystals were obtained through a one-step CVT process[39-41]. Among them, the Atomic radius of rare earth elements is large and difficult to be doped. The content of rare earth elements in the system is increased by using chlorides with low melting points to improve the success rate of doping. And when the amount of chloride increases, it will cause the doped MoS_2 film to grow thinner and smaller in size. (As shown in Figure S3). Here, we take Gd-doped monolayer MoS_2 as an example. Figure 4a presents the optical microscope image of a typical Gd-MoS_2 monolayer. It exhibits a well-defined triangular shape without grain boundaries, indicating the high quality of the as-grown Gd-MoS_2 monolayer. (The microscope image of Dy-MoS_2 monolayer in Figure S4 of the Supporting Information). Two characteristic Raman vibration modes of E^1_{2g} and A_{1g} of monolayer Gd-MoS_2 were collected by Raman spectroscopy using a 532 nm laser shown in Figure 4c. The E^1_{2g} mode represents the in-plane vibration of Mo-S atoms, while the A_{1g} mode is related to the out-plane vibration. The vibration peak position is almost consistent with that of undoped MoS_2, indicating that the doped ions have little effect on the lattice of the material, and the distance between the two vibration peaks is 19 cm^{-1}, which also indicates that a monolayer Gd doped MoS_2 has been prepared. Simultaneously, the Raman mapping in the illustration also shows the high-quality crystallinity of the material.

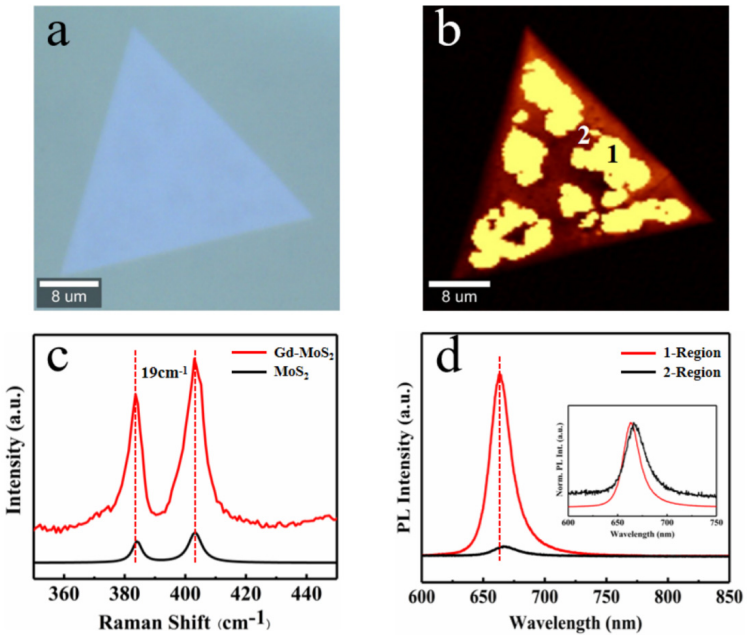

Figure 4. Synthesis of Gd-doped MoS_2 monolayer using CVT method. (a) A typical optical microscopy image of Gd-doped triangular MoS_2 monolayer. (b) PL-Mapping spectra of Gd-doped monolayer

Preprints (www.preprints.org) | NOT PEER-REVIEWED | Posted: 3 August 2023 doi:10.20944/preprints202308.0336.v1

MoS_2. According to luminescence intensity, the spectrum is divided into two regions: bright (1) and dark (2). (c) Raman spectra of Gd-MoS_2 and pure MoS_2 were obtained with a 532 nm laser. The distance between two vibration peaks is 19 cm-1. (d) The PL spectra of Gd-doped and undoped MoS_2 monolayer. Inset shows normalized spectra.

Analyze and characterize the PL performance of monolayer MoS_2 before and after Gd doping using a Raman spectrometer. It was found that the fluorescence luminescence of Gd-doped MoS_2 is not uniform (Figure 4d). In the PL mapping of monolayer MoS_2, there is a difference of more than ten times in the luminescence intensity of the two PL regions, bright region 1 and dark region 2. The luminescence intensity of the second region is consistent with the luminescence peak position and intensity of the undoped MoS_2. Due to the difference in the size of doped ions, it can affect the coordination environment in the matrix, leading to the formation of asymmetric fields[41-43]. The lower the symmetry of the substrate, the more uneven the crystal field environment around the doped ions, leading to an increase in electron coupling between the 4f energy level and higher electron configurations, resulting in an increase in the probability of f-f transition, specifically manifested in the significant luminescence intensity within the same triangular crystal.

However, due to the resolution of HR-TEM, the difference between Gd atoms and Mo cannot be diffraction in STEM images (Figure 5a). On the other hand, diffraction patterns indicate that the doped MoS_2 is a single crystal with high crystallinity, and the (100) plane spacing is about 0.271 nm, with a distance between two Mo atoms of about 0.316 nm. Compared to the plane spacing and atomic spacing of pure MoS_2, this confirms the lattice distortion phenomenon caused by doping large Gd atoms into the MoS_2 lattice. Figures 5d, e, and f show the elemental analysis results of the EDS spectrum, where Gd is uniformly distributed in the 2D MoS_2 crystal. The quantitative test results indicate that the doping ratio of Gd is about 3.19%.

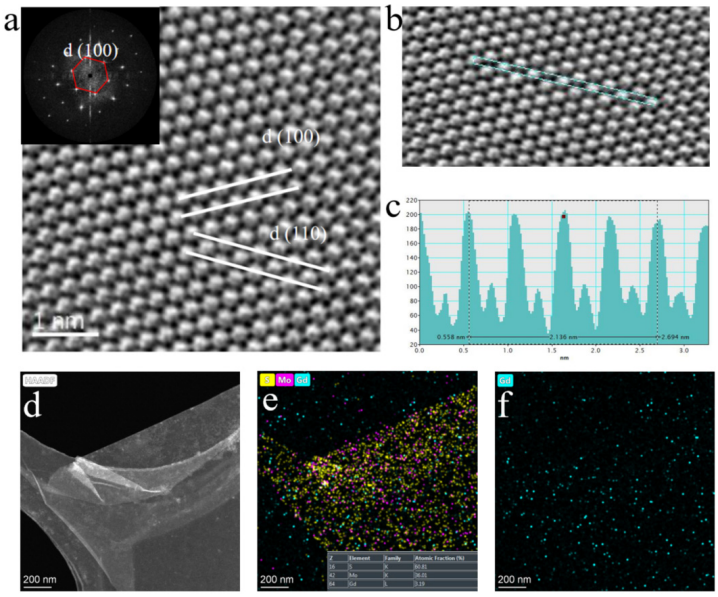

Figure 5. STEM and EDS test results of Gd-doped monolayer MoS^2. (a) Transmission electron microscope with a probe corrector (STEM) imaging. Scale bar: 1 nm. Inset: the corresponding FFT-diffraction patterns. (b) An enlarged view of the red rectangular area in (a). (c) The intensity line profile corresponding to the marked area in (b). (d) TEM-HAADF images of Gd-doped monolayer MoS_2. (e, f) Spatially resolved EDS maps collected from the same area in a Hf-MoS_2 monolayer for the Mo-K, S-K, and Gd-L lines.

Furthermore, in order to investigate the reasons for the enhancement of fluorescence intensity after Gd doping and the changing behavior of exciton transitions, transient absorption spectra and exciton lifetime tests were conducted on the sample using a pump detection system to analyze the luminescence kinetics of the sample. As shown in Figure 6b, we found that the absorption peaks of

Preprints (www.preprints.org) | NOT PEER-REVIEWED | Posted: 3 August 2023 doi:10.20944/preprints202308.0336.v1

A and B excitons in MoS_2 doped with Gd shifted red by about 2 nm, and the intensity was significantly enhanced, consistent with the luminescence intensity and peak position changes of the PL spectrum. Figure 6c, d shows that the lifetimes of excitons A and B are much longer than those of pure MoS_2, corresponding to the significant enhancement of PL strength after Gd doping. The defect capture process in various stages of exciton lifetime τ_1 has also significantly increased in length due to introducing more defects after doping and more electrons in rare earth elements. Exciton recombination process τ_2 and exciton annihilation process τ_3. Compared to before doping, the intensity of PL increased by many times, corresponding to a significant increase in PL intensity. However, due to the large size of rare earth elements, more defects are introduced after doping, resulting in poor crystal quality and lower PL intensity to Ti doping.

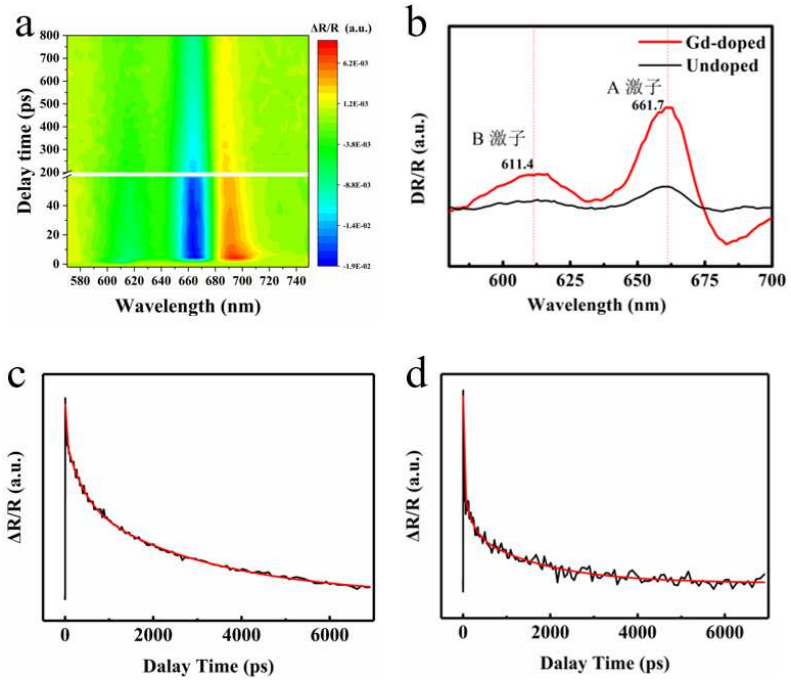

Figure 6. Time-resolved dynamics of the Gd-doped. (a) TR contour plot of Gd-doped MoS_2 monolayer on a mica substrate. (b) TR spectra extracted from (a) with the delay of 6.83 ps under the 532 nm laser excitation. (c, d) The TR kinetic curves of exciton resonance of A and B obtained through a triexponential fitting were extracted from (b).

Table 2. Tri-exponentially fitted Lifetimes results of A-exciton resonance for the Gd-doped and undoped monolayer MoS_2.

Exciton	Monolayer	τ_1 (ps)	τ_2 (ps)	τ_3 (ps)
A	Pristine	0.91	24.11	390.08
	Doped	14.3	384.28	3012.01

In addition, we also selected Ti (Our research group has previously reported the relevant work), Zr as the IVB group element (Figure S2, Supporting Information), and Dy as the rare earth element for monolayer MoS_2 doping experiments. It was found that the doping of the Zr element resulted in a two-fold decrease in PL performance. Tests showed that doping with electrons of different orbital energy levels affected their internal electronic transition behavior and enhanced their luminescence performance. Zr atoms had the same electronic energy levels as Mo atoms, with no transition behavior energy levels. After doping, only the effect of crystal quality deterioration resulted in a decrease in their luminescence performance[44-46]. As for the other rare earth element Dy, the doping effect is similar to that of Gd, but the luminescence effect of Dy-doped monolayer MoS_2 is only three times enhanced, which also indicates that the luminescence effect of Gd element doped with F orbitals in a semi-full state is evident. The data can be found in supporting literature.

Preprints (www.preprints.org) | NOT PEER-REVIEWED | Posted: 3 August 2023 doi:10.20944/preprints202308.0336.v1

4. Conclusions

In summary, the one-step CVT method was used to improve the phenomenon of uneven doping in monolayer TMDCs materials and successfully achieved the doping of Zr, Hf in transition IVB and VB families, as well as Gd, Dy elements in monolayer MoS_2. The doping behavior of elements was demonstrated through testing methods such as Raman, STEM, EDS, and XPS, which significantly enhanced the PL luminescence of Hf and Gd doped monolayer MoS_2 compared to pure MoS_2. Furthermore, the carrier dynamics tests reveal that the introduced O-X-S (X=Hf, Gd) units facilitate the radiative recombination and interact with the substrate, leading to the PLQY increase and giant PL enhancement. On the other hand, the PL enhancement and weakening of monolayer MoS_2 by doping elements can be roughly divided into two categories. It is speculated that the varying degrees of strain caused by element ions of different diameters on the original lattice will have different effects on the luminescent performance of the material. This provides reference and guidance for the future doping synthesis of TMDCs.

Supplementary Materials: The following supporting information can be downloaded at the website of this paper posted on Preprints.org.

Author Contributions: Conceptualization, Z.H. and Y.W.; methodology, H.Q. and L.L.; validation, Z.H. and B.Z.; formal analysis, B.Z.; investigation, H.L.; writing-original draft preparation, B.Z.; writing-review and editing, H.Q.; supervision, H.L.; project administration, Z.H.; funding acquisition, Y.W. All authors have read and agreed to the published version of the manuscript.

Acknowledgments: This work is supported by the NSFC (51972229, 518022185. The Key Research and Development Program of the Ministry of Science and Technology (GG20210301), National Defense Science and Technology 173 Program (2021-JCJQ-JJ-0639).

Conflicts of Interest: The authors declare that they have no conflicts of interest.

References

1. Ye M, Zhang D, Yap Y K. Recent advances in electronic and optoelectronic devices based on two-dimensional transition metal dichalcogenides[J]. *Electronics*, **2017**, *6(2)*: 43.
2. Jariwala D, Sangwan V K, Lauhon L J, et al. Emerging device applications for semiconducting two-dimensional transition metal dichalcogenides[J]. *ACS nano*, **2014**, *8(2)*: 1102-1120.
3. Wu M, Xiao Y, Zeng Y, et al. Synthesis of two-dimensional transition metal dichalcogenides for electronics and optoelectronics[J]. *InfoMat*, **2021**, *3(4)*: 362-396.
4. Cai Z, Shen T, Zhu Q, et al. Dual-Additive Assisted Chemical Vapor Deposition for the Growth of Mn-Doped 2D MoS_2 with Tunable Electronic Properties[J]. Small, 2020, 16(15): 1903181.
5. Chaves A, Azadani J G, Alsalman H, et al. Bandgap engineering of two-dimensional semiconductor materials[J]. *npj 2D Materials and Applications*, **2020**, *4(1)*: 29.
6. Tedstone A A, Lewis D J, O'Brien P. Synthesis, properties, and applications of transition metal-doped layered transition metal dichalcogenides[J]. *Chemistry of Materials*, **2016**, *28(7)*: 1965-1974.
7. Ma Z, Ren C, Wu Y, et al. Dopant-Induced Giant Photoluminescence of Monolayer MoS_2 by Chemical Vapor Transport[J]. *Advanced Materials Interfaces*, **2022**, *9(25)*: 2200431.
8. Pi X. Doping silicon nanocrystals with boron and phosphorus[J]. *Journal of Nanomaterials*, **2012**, *2012: 3-3*.
9. Li M, Wu X, Guo W, et al. Controllable p-type doping of monolayer MoS_2 with tantalum by one-step chemical vapor deposition[J]. *Journal of Materials Chemistry C*, **2022**, *10(19)*: 7662-7673.
10. Zhang J, Tian X, Liu M, et al. Cobalt-modulated molybdenum–dinitrogen interaction in MoS_2 for catalyzing ammonia synthesis[J]. *Journal of the American Chemical Society*, **2019**, *141(49)*: 19269-19275.
11. Wang Z, Wang W, Yang Y, et al. The structure and stability of molybdenum ditelluride thin films[J]. *International Journal of Photoenergy*, **2014**, *2014*.
12. Kochat V, Apte A, Hachtel J A, et al. Re doping in 2D transition metal dichalcogenides as a new route to tailor structural phases and induced magnetism[J]. *Advanced Materials*, **2017**, *29(43)*: 1703754.
13. Suh J, Park T E, Lin D Y, et al. Doping against the native propensity of MoS_2: degenerate hole doping by cation substitution[J]. *Nano letters*, 2014, *14(12)*: 6976-6982.

Preprints (www.preprints.org) | NOT PEER-REVIEWED | Posted: 3 August 2023 doi:10.20944/preprints202308.0336.v1

14. Suh J, Tan T L, Zhao W, et al. Reconfiguring crystal and electronic structures of MoS_2 by substitutional doping[J]. *Nature communications*, **2018**, *9(1)*: 199.
15. Lin X, Ni J. Charge and magnetic states of Mn-, Fe-, and Co-doped monolayer MoS_2[J]. *Journal of Applied Physics*, **2014**, *116(4)*.
16. Fang Q, Zhao X, Huang Y, et al. Structural stability and magnetic-exchange coupling in Mn-doped monolayer/bilayer MoS_2[J]. *Physical Chemistry Chemical Physics*, **2018**, *20(1)*: 553-561.
17. Ramasubramaniam A, Naveh D. Mn-doped monolayer MoS_2: An atomically thin dilute magnetic semiconductor[J]. *Physical Review B*, **2013**, *87(19)*: 195201.
18. Bai G, Yuan S, Zhao Y, et al. 2D layered materials of rare-earth Er-doped MoS_2 with NIR-to-NIR down-and up-conversion photoluminescence[J]. *Advanced Materials*, **2016**, *28(34)*: 7472-7477.
19. Zhang X, Lai Z, Tan C, et al. Solution-processed two-dimensional MoS_2 nanosheets: preparation, hybridization, and applications[J]. *Angewandte Chemie International Edition*, **2016**, *55(31)*: 8816-8838.
20. Vidya Y S, Lakshminarasappa B N. Influence of rare earth doping on microstructure and luminescence behaviour of sodium sulphate[J]. *Indian Journal of Materials Science*, **2014**, *2014*.
21. Ghosh S K, Srivastava C, Nath S, et al. Simple formation of nanostructured molybdenum disulfide thin films by electrodeposition[J]. *International Journal of Electrochemistry*, **2013**, *2013*.
22. Zhao Y, Ippolito S, Samori P. Functionalization of 2D Materials with Photosensitive Molecules: From Light-Responsive Hybrid Systems to Multifunctional Devices[J]. *Advanced Optical Materials*, **2019**, *7(16)*: 1900286.
23. Xie C, Yan F. Flexible photodetectors based on novel functional materials[J]. *Small*, **2017**, *13(43)*: 1701822.
24. Wang J, Zheng H, Xu G, et al. Controlled Synthesis of Two-Dimensional 1 T-$TiSe_2$ with Charge Density Wave Transition by Chemical Vapor Transport[J]. *Journal of the American Chemical Society*, **2016**, *138(50)*: 16216-16219.
25. Raza A, Qumar U, Haider A, et al. Liquid-phase exfoliated MoS_2 nanosheets doped with p-type transition metals: a comparative analysis of photocatalytic and antimicrobial potential combined with density functional theory[J]. *Dalton Transactions*, **2021**, *50(19)*: 6598-6619.
26. Sun C, Jiang Y, Cui M, et al. High-performance large-area quasi-2D perovskite light-emitting diodes[J]. *Nature communications*, **2021**, *12(1)*: 2207.
27. Li X, Chen C, Yang Y, et al. 2D Re-Based Transition Metal Chalcogenides: Progress, Challenges, and Opportunities[J]. *Advanced Science*, **2020**, *7(23)*: 2002320.
28. Yin X, Wang Q, Cao L, et al. Tunable inverted gap in monolayer quasi-metallic MoS_2 induced by strong charge-lattice coupling[J]. *Nature communications*, **2017**, *8(1)*: 486.
29. Azizi A, Wang Y, Stone G, et al. Defect Coupling and Sub-Angstrom Structural Distortions in $W_{1-x}Mo_xS_2$ Monolayers[J]. *Nano letters*, **2017**, *17(5)*: 2802-2808.
30. Tang B, Yu Z G, Huang L, et al. Direct n-to p-type channel conversion in monolayer/few-layer WS_2 field-effect transistors by atomic nitrogen treatment[J]. *ACS nano*, **2018**, *12(3)*: 2506-2513.
31. Wang S, Robertson A, Warner J H. Atomic structure of defects and dopants in 2D layered transition metal dichalcogenides[J]. *Chemical Society Reviews*, **2018**, *47(17)*: 6764-6794.
32. Wang Q, Lei Y, Wang Y, et al. Atomic-scale engineering of chemical-vapor-deposition-grown 2D transition metal dichalcogenides for electrocatalysis[J]. *Energy & Environmental Science*, **2020**, *13(6)*: 1593-1616.
33. Cui Q, Luo Z, Cui Q, et al. Robust and high photoluminescence in WS_2 monolayer through in situ defect engineering[J]. *Advanced Functional Materials*, **2021**, *31(38)*: 2105339.
34. Zheng B, Zheng W, Jiang Y, et al. WO_3–WS_2 vertical bilayer heterostructures with high photoluminescence quantum yield[J]. *Journal of the American Chemical Society*, **2019**, *141(30)*: 11754-11758.
35. Zhao J, Zhao W, Du W, et al. Dynamics of exciton energy renormalization in monolayer transition metal disulfides[J]. *Nano Research*, **2020**, *13*: 1399-1405.
36. Sun D, Rao Y, Reider G A, et al. Observation of rapid exciton–exciton annihilation in monolayer molybdenum disulfide[J]. *Nano letters*, **2014**, *14(10)*: 5625-5629.
37. Peng J, Yang D, Ren C, et al. Electronic properties and carrier dynamics at the alloy interfaces of $WS_{2x}Se_{2-2x}$ spiral nanosheets[J]. *Advanced Materials*, **2022**, *34(11)*: 2107738.
38. Luo Z, Zheng W, Luo N, et al. Photoluminescence lightening: extraordinary oxygen modulated dynamics in WS_2 monolayers[J]. *Nano Letters*, **2022**, *22(5)*: 2112-2119.
39. Chen P, Han W, Zhao M, et al. Recent advances in 2D rare earth materials[J]. *Advanced Functional Materials*, **2021**, *31(13)*: 2008790.

Preprints (www.preprints.org) | NOT PEER-REVIEWED | Posted: 3 August 2023 doi:10.20944/preprints202308.0336.v1

40. Zhang Z, Zhao H, Zhang C, et al. Rare-earth-incorporated low-dimensional chalcogenides: Dry-method syntheses and applications[J]. *InfoMat*, **2020**, *2(3)*: 466-482.
41. Saponjic Z V, Dimitrijevic N M, Poluektov O G, et al. Charge separation and surface reconstruction: A Mn^{2+} doping study[J]. *The Journal of Physical Chemistry B*, **2006**, *110(50)*: 25441-25450.
42. Dash A, Sarkar S, Adusumalli V N K B, et al. Microwave synthesis, photoluminescence, and photocatalytic activity of PVA-functionalized Eu^{3+}-doped BiOX (X= Cl, Br, I) nanoflakes[J]. *Langmuir*, **2014**, *30(5)*: 1401-1409.
43. Karasulu B, Emge S P, Groh M F, et al. Al/Ga-doped $Li_7La_3Zr_2O_{12}$ garnets as Li-ion solid-state battery electrolytes: atomistic insights into local coordination environments and their influence on ^{17}O, ^{27}Al, and ^{71}Ga NMR spectra[J]. *Journal of the American Chemical Society*, **2020**, *142(6)*: 3132-3148.
44. Zhou J, Zheng G, Liu X, et al. Defect engineering in lanthanide doped luminescent materials[J]. *Coordination Chemistry Reviews*, **2021**, *448*: 214178.
45. Xiong P, Huang B, Peng D, et al. Self-recoverable mechanically induced instant luminescence from Cr^{3+}-doped $LiGa_5O_8$[J]. *Advanced Functional Materials*, **2021**, *31(19)*: 2010685.
46. Piao Y, Meany B, Powell L R, et al. Brightening of carbon nanotube photoluminescence through the incorporation of sp^3 defects[J]. *Nature chemistry*, **2013**, 5(10): 840-845.

Disclaimer/Publisher's Note: The statements, opinions and data contained in all publications are solely those of the individual author(s) and contributor(s) and not of MDPI and/or the editor(s). MDPI and/or the editor(s) disclaim responsibility for any injury to people or property resulting from any ideas, methods, instructions or products referred to in the content.